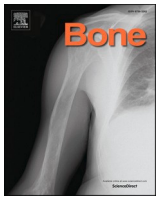
Bone 150 (2021) 116008



Contents lists available at ScienceDirect

Bone

journal homepage: www.elsevier.com/locate/bone



Full Length Article



Impaired soft and hard callus formation during fracture healing in diet-induced obese mice as revealed by 3D contrast-enhanced computed tomography imaging

Carlos Marin [a,b,c], Jolien Tuts [c], Frank P. Luyten [a,b], Katleen Vandamme [b,c,1], Greet Kerckhofs [b,d,e,f,*,1]

[a] Skeletal Biology and Engineering Research Center, Department of Development and Regeneration, KU Leuven, Leuven, Belgium
[b] Prometheus – Division of Skeletal Tissue Engineering Leuven, KU Leuven, Leuven, Belgium
[c] Biomaterials – BIOMAT, Department of Oral Health Sciences, KU Leuven, Leuven, Belgium
[d] Department of Material Science and Engineering, KU Leuven, Leuven, Belgium
[e] Biomechanics lab, Institute of Mechanics, Materials, and Civil Engineering, UCLouvain, Louvain-la-Neuve, Belgium
[f] Institute for Experimental and Clinical Research, UCLouvain, Woluwe, Belgium

ARTICLE INFO

Keywords:
Fracture healing
Diet-induced obesity
Bone repair
Contrast-enhanced computed tomography
Hyperglycemia
Periosteum-derived cells

ABSTRACT

The impact of diabetes mellitus on bone fracture healing is clinically relevant as the patients experience delayed fracture healing. Even though efforts have been made to understand the detrimental effects of type 2 diabetes mellitus (T2DM) on the fracture healing process, the exact mechanisms causing the pathophysiological outcomes remain unclear. The aim of this study was to assess alterations in bone fracture healing (tibial fracture surgery, intramedullary pinning) of diet-induced obese (DIO) mice, and to investigate the *in vitro* properties of osteochondroprogenitors derived from the diabetic micro-environment. High-resolution contrast-enhanced micro-focus X-ray computed tomography (CE-CT) enabled a simultaneous 3D assessment of the amount and spatial distribution of the regenerated soft and hard tissues during fracture healing and revealed that osteogenesis as well as chondrogenesis are altered in DIO mice. Compared to age-matched lean controls, DIO mice presented a decreased bone volume fraction and increased callus volume and adiposity at day 14 post-fracture. Of note, bone turnover was found altered in DIO mice relative to controls, evidenced by decreased blood serum osteocalcin and increased serum CTX levels. The *in vitro* data revealed that not only the osteogenic and adipogenic differentiation of periosteum-derived cells (PDCs) were altered by hyperglycemic (HG) conditions, but also the chondrogenic differentiation. Elevated PPARγ expression in HG conditions confirmed the observed increase in differentiated adipocytes *in vitro*. Finally, chondrogenesis-related genes COL2 and COL10 were downregulated for PDCs treated with HG medium, confirming that chondrogenic differentiation is compromised *in vitro* and suggesting that this may affect callus formation and maturation during the fracture healing process *in vivo*. Altogether, these results provide novel insights into the alterations of long bone fracture repair and suggest a link between HG-induced dysfunctionality of osteochondroprogenitor differentiation and fracture healing impairment under T2DM conditions.

1. Introduction

Bone healing after trauma is a complex and long process in which many different mechanical and biological conditions must be met for proper tissue repair [1]. A compromised micro-environment, such as a diabetic one, could alter these conditions at any of the described phases of the fracture repair process, *i.e.* inflammation, repair and remodeling [1]. Currently, diabetes mellitus (DM) is considered a worldwide epidemic, predicted to be the seventh leading cause of death in the year 2030 [2]. Particularly, type 2 diabetes mellitus (T2DM) is a common comorbidity of obesity and it is characterized by hyperglycemia, resulting from insulin resistance and malfunction of the β-cells in the

* Corresponding author at: Biomaterials, Biomechanics Lab, Institute of Mechanics, Materials, and Civil Engineering, UCLouvain, Louvain-la-Neuve, Belgium.
E-mail address: greet.kerckhofs@uclouvain.be (G. Kerckhofs).
[1] Shared last authorship.

https://doi.org/10.1016/j.bone.2021.116008
Received 14 January 2021; Received in revised form 7 May 2021; Accepted 10 May 2021
Available online 14 May 2021
8756-3282/© 2021 Published by Elsevier Inc.

pancreas [3]. Among its known complications, this metabolic disease also affects the skeletal system, altering bone homeostasis, with an increased fracture risk and impaired fracture healing [4–7]. Bone fracture healing experiments report that rodents with high-fat diet (HFD)-induced T2DM present compromised bone biomechanical properties, altered vascular, adipose and mineralized tissue in the fracture callus, and upregulated levels of PPARγ expression [6,8].

A valuable tool used to investigate the negative effects of T2DM on bone fractures is X-ray microfocus computed tomography (microCT). By applying this technique, Tencerova et al. [9] reported lower trabecular bone mass and cortical thickness in a model of C57BL/6J mice fed with a HFD for 12 weeks [9]. Similarly, Brown et al. [6] revealed through microCT that fracture callus volume at day 21 post-fracture surgery was smaller, that woven bone area was decreased and that peak bone volume was delayed in HFD-fed mice when compared to control animals [6]. In line with these findings, another study reported delayed new bone defect filling (only 21% compared to 57% in controls) 12 weeks post-operatively of a subcritical femoral defect model in T2DM rats [8]. In these studies, however, microCT analysis was limited to the visualization of the mineralized tissues within the fracture callus. A powerful recent addition to microCT is the use of contrast-enhancing staining agents. High-resolution contrast-enhanced microCT (CE-CT) allows for the visualization and quantification of not only mineralized, but also soft tissues [10–13] that otherwise cannot be assessed with standard absorption mode microCT. For cartilaginous tissue, the iodine-based anionic agent ioxaglate (Hexabrix™) has been used previously in order to assess the proteoglycan content [14]. In a study from Kerckhofs et al. [14], a mouse model of osteoarthritis was used to investigate the quality and structure of cartilaginous tissue by CE-CT, and the authors compared CE-CT's applicability, non-destructive nature and complementary value to standard histomorphometry [14]. Additionally, very recent studies have used CE-CT to assess other components of skeletal tissues such as the vasculature and adipose tissue in the bone marrow of obese mouse models [15,16]. Thus, it was demonstrated that CE-CT is a useful and accurate technology for the 3D visualization and quantification also of soft tissues. In this study, we used this characterization method to determine how T2DM was impairing bone repair, through the simultaneous assessment of different skeletal tissues within the fracture callus of T2DM mice.

The transformations that different skeletal tissues undergo during fracture healing are dependent on the functional state of the osteochondroprogenitor cells recruited during bone repair [6,17]. Various studies have demonstrated that the normal functionality of osteoprogenitor cells is compromised under *in vitro* conditions of hyperglycemia (HG) [18,19]. More specifically, it is suggested that biological pathways, like the BMP signaling pathway and the PI3K/Akt pathway, are affected by HG, impairing cellular processes such as osteogenic and adipogenic differentiation [19,20]. The preferred cell type that has previously been used to assess the effects of HG on cellular functionality and to evaluate bone formation and regeneration is the bone marrow mesenchymal stem cell (BM-MSC) [18,21,22]. However, studies have shown that the periosteum represents a clinically more relevant source for the isolation of osteoprogenitors, since it relates more closely to the endochondral bone repair process [23,24]. Periosteum-derived cells (PDCs) are proven to have a high differentiation potential towards the osteogenic, adipogenic and chondrogenic lineages, strong proliferation capacity and proangiogenic potential [24]. Information regarding their functionality in a compromised micro-environment such as diabetes is currently lacking in literature. We therefore studied the effect that an *in vitro* HG environment exerts on mouse PDCs isolated from the diabetic micro-environment. These results were used to complement the findings obtained *in vivo* using CE-CT and allowed us to gain insight into the biology of these osteochondroprogenitors under T2DM conditions and their share in the fracture healing process.

2. Materials and methods

2.1. Animals

Animal experimentation was approved by the Ethics Committee of the University of Leuven (P101/2014) and was in compliance with the ARRIVE guidelines (https://arriveguidelines.org/). 6-week-old C57BL/6 male mice were obtained from Janvier Labs (Le Genest-Saint-Isle, France). Four mice per cage were housed and allowed to acclimatize for 2 weeks before the start of the experiments. A 12:12 h light-dark cycle was implemented, and room temperature was kept at 22 °C. Food and water were available *ad libitum*. Next, 8-week-old mice were randomly divided into 2 diet groups: a low-fat diet (LFD, 11 kcal% fat - age-matched lean (AML) group, $n = 7$) and high-fat diet (HFD, 60 kcal% fat - diet-induced obese (DIO) group, $n = 6$) group. The diets (HFD: D12492, Research Diets, Inc. – New Brunswick, NJ, USA, open source; LFD: R/M-H, Ssniff®, Soest, Germany) were administered for a period of 14 weeks, allowing the DIO animals to reach a diabetic condition by the age of 22 weeks. In order to take into account the potential changes in bone tissue due to ageing, young non-diabetic 8-week-old mice were included as a control group (young (YNG) group, $n = 8$). Body weight and blood glucose levels in fasting conditions were determined at the end of the experiment.

2.2. Tibial fracture surgery

Mice underwent tibial fracture surgery (in-house protocol) 14 weeks after the start of the LFD/HFD administration. Briefly, mice were anesthetized intraperitoneally with a mixture of ketamine/xylazine (ketamine 80 mg/kg + xylazine 10 mg/kg). A longitudinal skin incision was made on the anterior side of the tibia to ensure the exposition of the knee joint and a 25G needle was inserted transversally underneath the fracture site (mid-diaphyseal level), to allow for its full exposure. Subsequently, a 26G needle was inserted into the tibia *via* the proximal articular surface to access the marrow cavity through the epiphysis. The 26G needle was replaced by a 27G needle, inserted deeper and parallel to the longitudinal bone axis, and after its retraction the fracture was induced using rotary instrumentarium equipped with a diamond cutting disk. Next, the fracture was semi-stabilized by re-introducing the 27G needle, functioning as an intramedullary fixating pin. Finally, the fibula was cut at the level of the fracture site to avoid displacement of the fractured tibia's halves. After skin suture and wound disinfection, the mice were monitored for 2 h post-surgery. At day 14 post-surgery, mice were euthanized, and dissected bones were fixed in 2% paraformaldehyde for 16 h and changed to phosphate-buffered saline (PBS) for storage at 4 °C.

2.3. CE-CT acquisition, image analysis and histology

In order to simultaneously visualize the different skeletal tissues (bone, mineralized cartilage, unmineralized cartilage and adipocytes), all bone samples ($n = 6$–8 per group) were immersed for 2 weeks in a solution of Hexabrix 320 diluted 4/5 in PBS. Subsequently, fractured tibias were scanned at 3.5 μm voxel size using the NanoTom M device (GE Measurement and Control Solutions, Germany). The system's source was set to 60 kV and 210 μA. An aluminum filter of 0.1 mm was used. The system scanning settings were: exposure time 500 ms, frame averaging 1 and skip 0, and 2400 radiographs, which allowed for a scanning time of 20 min per sample. The resulting images were analyzed with CTAn software (Bruker MicroCT, Kontich, Belgium) and we selected in length approximately 2.5 mm of the fracture callus area. First, a region of interest (ROI) was manually drawn around the entire callus area (*i.e.* ROI.1). Then, an additional ROI was manually drawn fitting the cortical bone (*i.e.* ROI.2) and this ROI was excluded from ROI.1 to ensure the quantification of tissue only from the callus. Using these cortex-free cross-sections (Fig. 1 – ROI.3), quantification proceeded as follows.

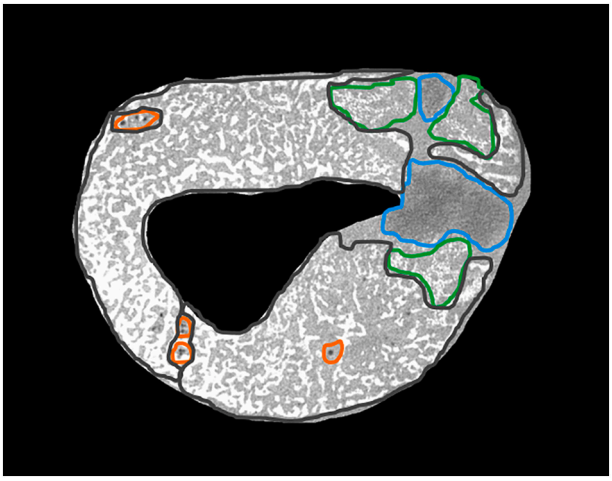


Fig. 1. CE-CT representative cross-section image of the hexabrix-stained fracture callus area, denoting newly-formed bone (encircled in dark gray – ROI.3), unmineralized cartilage (encircled in blue – ROI.4), mineralized cartilage (encircled in green – ROI.5), and adipocytes (encircled in orange – ROI.6). (For interpretation of the references to colour in this figure legend, the reader is referred to the web version of this article.)

Otsu segmentation was used to binarize ROI.3 (Otsu [25]), and noise removal was applied by carrying out a closing operation (round kernel, radius 1, 3D space) and a double despeckling step (removal of black and white speckles respectively), as described previously [26]. 3D analysis of the processed datasets was performed, which allowed obtaining the total callus volume. Regarding the tissues of interest within the fracture callus, ROIs specific for each of these were manually delineated based on the differences in grayscale (for unmineralized cartilage – ROI.4) and in structure (*i.e.* porous structure for mineralized cartilage – ROI.5, and spherical structure for adipocytes – ROI.6) (Fig. 1).

These differences in tissue structure were verified later through histological assays. Similar noise removal as mentioned before, manual segmentation and 3D analysis were performed on the different ROIs to calculate the volume of the different skeletal tissues relative to the total callus volume (BV/TV: bone volume fraction (%); MCV/TV: mineralized cartilage volume fraction (%); UCV/TV: unmineralized cartilage volume fraction (%); AV/TV: adipocyte volume fraction (%)). Finally, the resulting binarized datasets were used to generate 3D renderings using CTvox software (Bruker MicroCT, Kontich, Belgium).

Following CE-CT scanning, the bone samples were decalcified in 35 ml of 0.5 M EDTA/PBS solution (pH 7.3) for a period of 1 week (a total of 7 changes) at 4 °C. Then, samples were dehydrated, embedded in paraffin and sectioned at 5 μm. Histological stainings Alcian Blue and Masson Trichrome were carried out to assess the different skeletal tissues within the fracture callus of the different groups.

2.4. Isolation and expansion of mPDCs

Murine PDCs (mPDCs) were isolated from all non-fractured femora and tibiae of YNG, AML and DIO mice. Cell isolation was performed by enzymatic digestion following an in-house protocol [24]. Briefly, bones were dissected free of muscle under sterile conditions, by taking care not to damage the periosteum. Next, to prevent the release of non-periosteal cells by enzymatic digests, the bone epiphyses were embedded in 5% low melting point agarose. The enzymatic digestion of the fibrous matrix was done by incubating bones in a collagenase-dispase mix (3 mg/ml collagenase + 4 mg/ml dispase in α-Minimum essential medium "α-MEM" - Gibco, Brooklyn, NY, USA - L-glutamine + Ribonucleosides + Deoxyribonucleosides, low glucose concentration 5.5 mM, supplemented with 10% fetal bovine serum (FBS) and 1% penicillin/streptomycin) in a shaking water bath at 37 °C for 10 min. A second enzymatic digestion was carried out for 50 min to obtain the mPDCs. Cells from 3 animals were pooled together and plated in a T25 flask containing α-MEM medium. Cells were expanded and used at passage 2–3. For all *in vitro* experiments, three biological replicates (cell pools) were used unless indicated otherwise.

2.5. Cellular characterization of mPDCs

To assess the effect of HG on mPDCs, cells were cultured in glucose concentrations considered normoglycemic ("NG" - 5.5 mM) or HG (25 mM), according to standard cell culture systems described in literature [18,19].

Unless indicated otherwise, three days prior the start of the *in vitro* assays (D_{-3}), mPDCs were seeded and switched from expansion medium (α-MEM) to NG-Dulbecco's Modified Eagle Medium ("DMEM" - 2 mM glutaMAX-1 + 5.5 mM D-glucose, Gibco, Brooklyn, NY, USA - with 10% FBS and 1% penicillin/streptomycin), for habituation to the new medium used during the time of experimentation. At day 0 (D_0), cells were divided into two groups: one group was maintained in NG-DMEM and the other group was switched to HG-DMEM. Cells were cultured at 37 °C under 5% CO_2.

2.5.1. Viability and proliferation

Cells were seeded in 24-well plates at a density of 1×10^4 cells per well. Outcome parameters we evaluated at days 0, 2, 4, 7 and 10. In order to measure the viability of the mPDCs, the metabolic activity was evaluated using the PrestoBlue cell viability reagent (Invitrogen, Frederick, MD, USA). The optical density of samples and blank controls was measured at a wavelength of 570 nm. In order to assess the proliferative capacity of the mPDCs under NG and HG conditions, a PicoGreen DNA quantification assay (Quant-iT PicoGreen dsDNA kit, Life Technologies – Eugene, Oregon, USA) was carried out. The optical density of samples, blank controls and a Lambda DNA standard curve was measured using an excitation wavelength of 480 nm and emission of 520 nm.

2.5.2. Osteogenic differentiation

mPDCs were seeded in 24 well-plates at a density of 3×10^4/well. At D_1, osteogenic inducers were added. The osteogenic medium was composed of DMEM + 50 μg/ml L-ascorbic acid + 10 mM β-glycerophosphate. After 14 days (D_{14}) of culture in osteogenic NG *vs* HG medium, staining for extracellular alkaline phosphatase (ALP) was carried out, using the BM Purple AP substrate precipitating reagent (Sigma, St. Louis, Missouri, USA). In addition, the ALP activity of the mPDCs was quantified. Briefly, a mix of cellular extract (obtained by following the same steps as the DNA quantification assessment, previously mentioned), ALP buffer and paranitrophenyl phosphate solution (Pnpp 15 nM in MgCl2 2 mM) was placed in a water bath at 37 °C. The reactions were stopped for all samples 15 min after the start of the incubation, using NaOH 0.1 M. Then, the absorbance of samples, blanks and standard curves (prepared with paranitrophenol) was measured using a wavelength of 410 nm. The mineralization capacity of the mPDCs was evaluated at D_{14} by Alizarin Red staining (2% Alizarin Red S solution - Sigma, St. Louis, Missouri, USA; quantification by destaining with 10% hexadecylpyridinium chloride monohydrate - Sigma). The optical density was measured using a wavelength of 540 nm.

2.5.3. Adipogenic differentiation

mPDCs pools were seeded in 24-well plates at a density of 3×10^4 cells/well. Adipogenic inducers were added at D_1. The adipogenic medium was composed of DMEM + 10 nM dexamethasone + 10 μg/ml human insulin + 50 μM indomethacin + 500 nM IBMX. At D_{14}, Oil Red-O staining (60% Oil Red-O (Sigma) in Milli-Q water) was performed. Quantification was done using 100% isopropanol and the optical density was measured at a wavelength of 500 nm. Isopropanol blanks were used as controls.

2.5.4. Chondrogenic differentiation

Differentiation towards chondrocytes was achieved by culturing cells in high-density micromasses. To obtain the micromasses, 2×10^5 cells were resuspended in 10 μl of DMEM, and the process was followed as described previously [27]. After 28 days, quantification of glycosaminoglycans by 1% Alcian Blue (Sigma) staining was performed. Subsequently, micromasses were incubated overnight with 6 M guanidine hydrochloride (Sigma), and the optical density was measured using a wavelength of 630 nm.

2.5.5. RNA extraction and reverse-transcription quantitative PCR

Total RNA from cultured mPDCs was extracted using the Qiagen RNeasy Extraction Kit (Qiagen, Hilden, Germany) and quantified using the NanoDrop ND-1000 Spectrophotometer (Thermo Scientific, Waltham, Massachusetts, USA). Next, complementary DNA (cDNA) was synthesized by means of reverse transcription of 200 ng of total RNA, using RevertAid™ H Minus First Strand cDNA Synthesis Kit + Oligo(dT) 18 as a primer (Fermentas - Thermo Scientific). RNA-specific amplification was carried out through SYBR Green quantitative polymerase chain reaction (qPCR) primers. The qPCR was cycled in a Rotor-Gene sequence detector as follows: 95 °C for 3 min, 40 cycles of 95 °C for 3 s, and 60 °C for 60 s. Expression levels were analyzed using the $2^{-\Delta Ct}$ method and normalized for the expression of the housekeeping gene β-actin. Specific forward and reverse oligonucleotide primers used are shown below in Table 1.

2.6. Blood serum biomarkers of bone turnover

Blood samples from 11 to 13 animals per group were collected before euthanasia and serum was obtained 2 h post-collection. Serum osteocalcin (OC) and serum C-terminal telopeptide of type 1 collagen (CTX) levels were measured using ELISA kits (mouse Osteocalcin ELISA kit - Immunotopics, Inc.; RatLapsTM CTX-I EIA – Immunodiagnostic systems, PLC).

2.7. Statistical analysis

Data for all parameters were expressed as group means ± standard deviation. Student's *t*-test were used for the *in vivo* data for comparison DIO *vs* AML and AML *vs* YNG. For the *in vitro* part, Student's t-test were used to evaluate differences (i) between the groups (DIO *vs* AML and AML *vs* YNG – unpaired *t*-tests) and (ii) within groups (NG *vs* HG – paired t-tests). To account for potential Type I errors during the statistical analysis of the *in vitro* section, the Bonferroni correction was applied (Statistical significance achieved when $p < [0.05 / (n^\circ \text{ of statistical tests} = 7)]$, *i.e.* $p < 0.007$). All statistical analyses were performed using GraphPad PRISM (GraphPad software, La Joya, CA, USA).

3. Results

3.1. Physiological parameters are altered in DIO mice

When compared to the AML controls, the DIO mice evidenced a significant 2-fold increase in body weight (Fig. 2A). Fasting blood glucose levels showed a 2.4-fold increase in DIO mice compared to their age-matched counterparts (Fig. 2B). When comparing YNG and AML mice for these parameters, only body weight was significantly increased in AML.

Table 1
Forward and reverse primer sequences of target genes.

Gene	Forward primer	Reverse primer
RUNX2	TCCCCATCCATCCACTCCAC	GTTCTGAAGCACCTGCCTGG
PPARγ	CCCAATGGTTGCTGATTACAAA	AATAATAAGGTGGAGATGCAGGTTCT
SOX9	GAAGAACGGACAAGCGGAGG	GGACCCTGAGATTGCCCAGA
COL2	TCATCTTGCCGCATCTGTGTG	CCCTTTGGCCCTAATTTTCCACT
COL10	TCCCAGCACCAGAATCTATCTGA	TTATGCCTGTGGGGCGTTTGG
MEF2C	CCGATCCCGACTCCTCTTAT	TGGACACTGGGATGGAGACT

3.2. Significantly more cartilaginous and adipose tissue is observed in the DIO fracture callus

CE-CT scanning revealed that most DIO fractures did not bridge successfully 14 days post-surgery and the callus volume was slightly higher in comparison with the AML callus volume, though this difference was not significant. The callus volume of YNG mice was significantly smaller than the age-matched controls (Fig. 3A). Newly-formed trabecular BV/TV showed a trend to be decreased in DIO mice as compared to AML mice. However, AML mice evidenced a lower BV/TV in relation to the YNG group (Fig. 3B).

Meanwhile, the cartilage volume fraction (mineralized and unmineralized) was higher in the DIO callus in comparison to AML (Fig. 3C–D), suggesting a slower progression of the fracture repair process in the obese animals. The MCV/TV was significantly higher for DIO mice when contrasted to the AML group, which had, in turn, a significantly higher MCV/TV than their younger counterparts. It is important to note that the YNG callus had little to no unmineralized cartilage (Fig. 3D), suggesting that the fracture healing process in this group developed at a faster pace than in the AML group. Lastly, the differences in adipose tissue were significant between the fracture calluses of the DIO and AML mice (Fig. 3E), with a near to 5-fold higher volume fraction of adipose tissue in the DIO callus. Fig. 3F illustrates the composition of the callus for each group. 3D renderings of a representative CE-CT dataset per group show the tissue volume differences between the groups (Fig. 3G).

A comparison between the CE-CT images and histological sections stained with Alcian Blue and Masson Trichrome of YNG, AML and DIO fracture calluses is presented in Fig. 4. Skeletal tissue types detected *via* CE-CT were verified by direct comparison to standard 2D histology on the same samples. Cartilaginous tissue was detected in the Alcian Blue sections, especially in the AML and DIO fracture calluses (Fig. 4F and J). It can be seen that for both DIO and AML mice, a large number of hypertrophic chondrocytes (stained light purple/blue) were still present at Day 14 post-surgery in the callus (Fig. 4H and L). The YNG callus, though, showed a considerably lower number of chondrocytes, and a much larger area of the callus occupied by thick trabecular bone-like structures (stained deep purple/blue, Fig. 4C and D) when compared to the age-matched controls (Fig. 4G and H). Fig. 4J–L evidence a higher presence of cartilaginous tissue in the DIO callus compared to the AML callus (Fig. 4F–H), detected as well by means of CE-CT (Fig. 4E and I).

3.3. DIO-PDCs display altered trilineage differentiation potential in vitro

The proliferation capacity of the DIO-PDCs was significantly decreased in HG culture conditions compared to normoglycemic ones (Fig. 5A). This was also observed for the YNG cells, whereas the difference between NG and HG conditions was not significantly different for AML-PDCs. Furthermore, DNA quantification (Fig. 5B) revealed that hyperglycemia substantially affected the viability of YNG-PDCs at an early point in the *in vitro* culture (from day 2 onwards). Under both culture conditions, but especially when treated with NG medium (Fig. 5A–B), the proliferation of YNG-PDCs was significantly higher than that of the AML-PDCs at all studied timepoints. This was not the case when the latter were compared with the PDCs isolated from the diabetic micro-environment.

ALP and Alizarin Red stainings demonstrated that a HG condition (compared to NG) negatively affects the osteogenic differentiation and mineralization capacity of all mPDC groups studied (Fig. 6A–B and lowest panel). An exception can be observed for the Alizarin Red staining of AML-PDCs, which showed a trend towards increased mineralization (without statistical significance) under HG condition compared to the NG condition (Fig. 6B and lowest panel). Moreover,

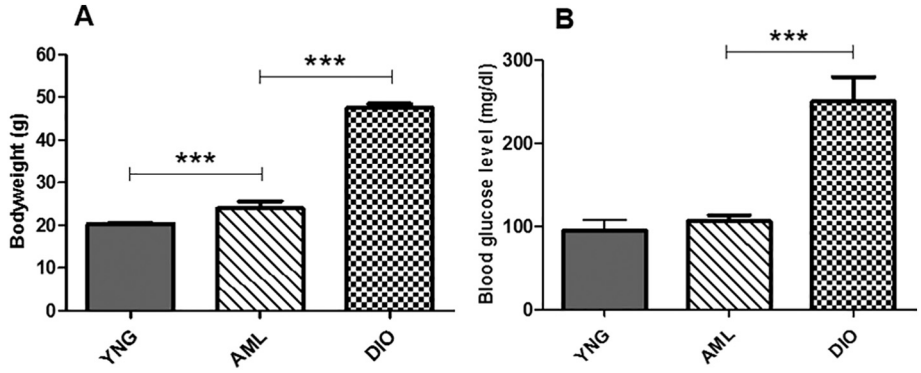


Fig. 2. A: Body weight and B: fasting blood glucose of YNG, AML and DIO mice. ***p < 0.001. n = 6–8 per group.

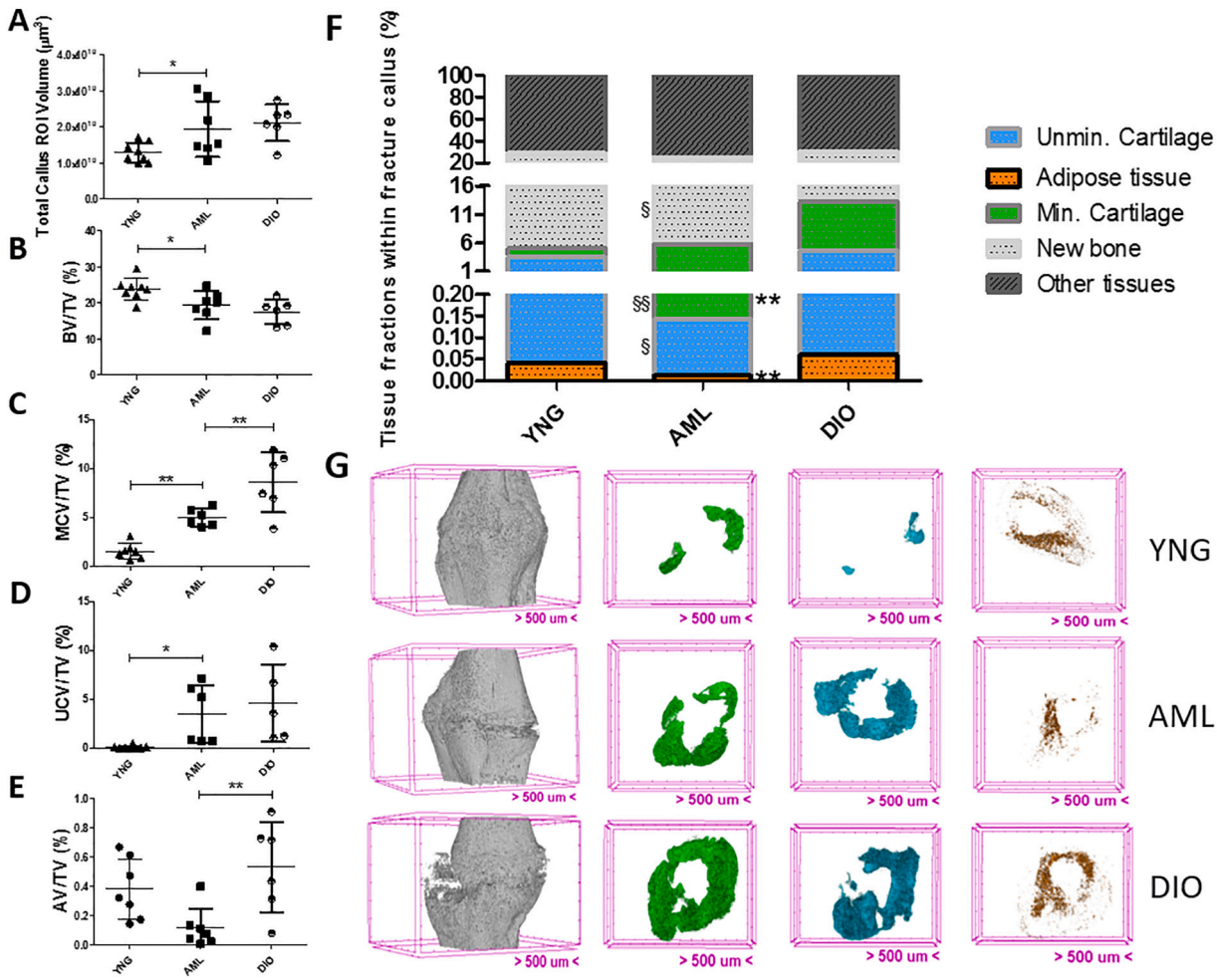


Fig. 3. A: CE-CT-based quantification of the fracture callus volume; B: tissue volume fractions of newly-formed bone; C: mineralized cartilage; D: unmineralized cartilage and E: adipocyte tissue of YNG, AML and DIO mice. F: Fraction of skeletal tissues (%) present within the fracture callus for each mouse group. G: 3D renderings of the skeletal tissues involved in the fracture healing process, from left to right: newly-formed bone (gray); mineralized cartilage (green); unmineralized cartilage (blue) and adiposity (orange). Statistical significance for YNG *vs* AML pair: § = p < 0.05 and §§ = p < 0.01; Statistical significance for AML *vs* DIO pair: * = p < 0.05 and ** = p < 0.01. n = 6–8 per group. (For interpretation of the references to colour in this figure legend, the reader is referred to the web version of this article.)

significant accumulation of lipid droplets, stained with the Oil Red-O assay, could be observed for all mPDCs groups under HG culture conditions (Fig. 6C and lowest panel). Finally, chondrogenic differentiation was found to be impaired by hyperglycemia in all mPDCs groups (Fig. 6D and lowest panel).

When comparing the ALP activity between groups (Fig. 6, lowest panel), a decreased activity was found for both NG and HG conditions of DIO-PDCs compared to their control counterparts, but these differences were not statistically significant. There were no differences between the YNG *vs* AML comparisons. DIO-PDCs were significantly less mineralized when compared to AML cells, for both culture conditions (Fig. 6, lowest panel – Alizarin Red staining). DIO-PDCs also displayed a significantly

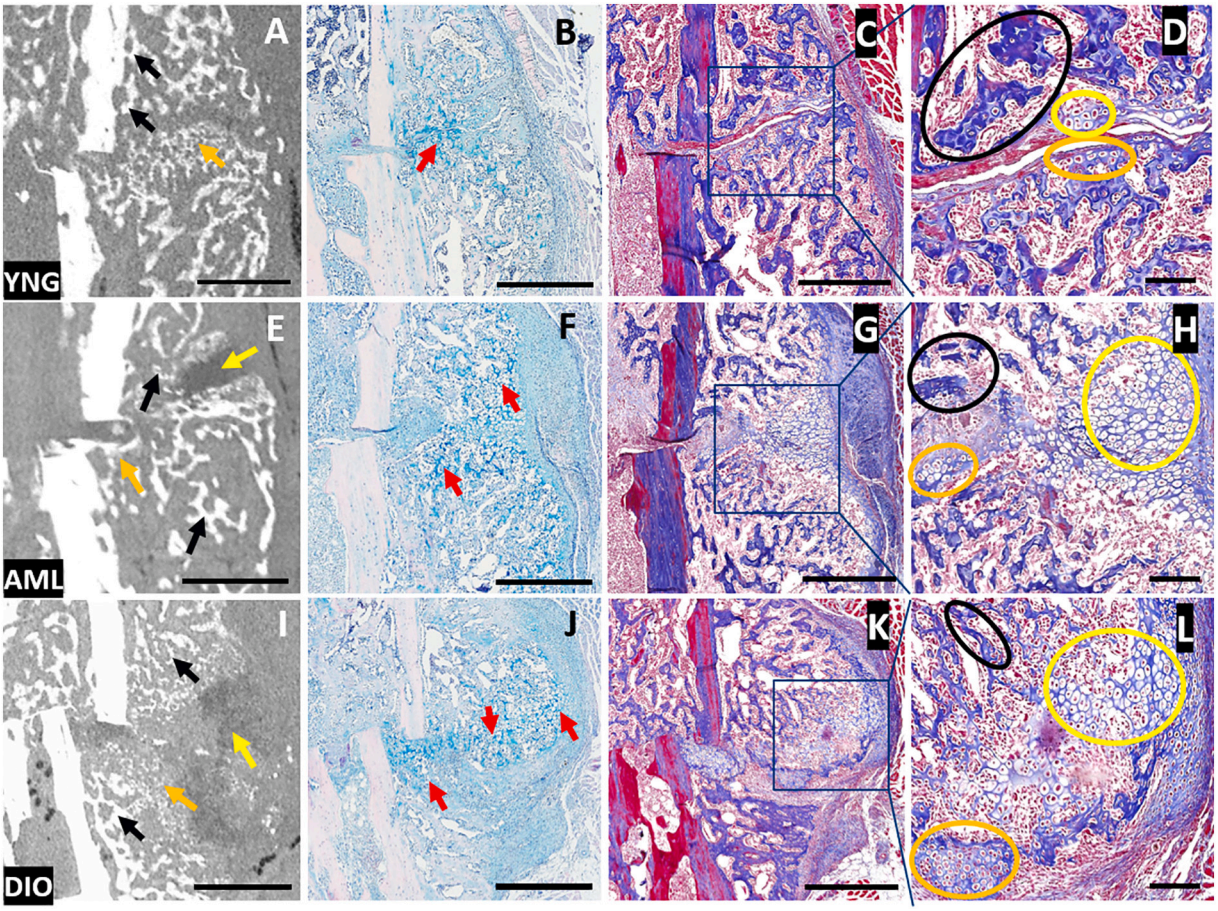


Fig. 4. Representative CE-CT images of YNG (A), AML (E) and DIO (I) fracture calluses stained with Hexabrix. Black, orange and yellow arrows represent newly-formed bone, mineralized cartilage and unmineralized cartilage, respectively. Histological sections stained with Alcian Blue (YNG: B, AML: F and DIO: J) and Masson Trichrome (YNG: C, AML: G and DIO: K) of fracture calluses from YNG, AML and DIO mice. The red arrows represent the positively stained cartilaginous tissue. Black boxes contain the area magnified in D (YNG), H (AML) and L (DIO). Black, orange and yellow circles represent newly-formed bone, mineralized cartilage and unmineralized cartilage, respectively. Scale bars = 500 μm except for D, H and L, with scale bars = 100 μm. $n = 6–8$ per group. (For interpretation of the references to colour in this figure legend, the reader is referred to the web version of this article.)

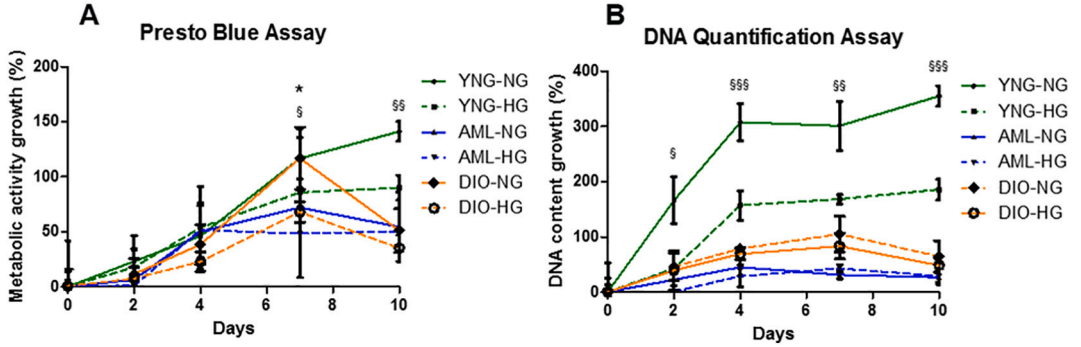


Fig. 5. Proliferation and viability assessment of YNG-, AML- and DIO-PDCs under NG and HG treatments, by A: Presto Blue and B: DNA quantification assays. Statistical significance for YNG-NG *vs* YNG-HG pair: § = $p < 0.05$; §§ = $p < 0.01$; §§§ = $p < 0.01$; Statistical significance for DIO-NG *vs* DIO-HG: * = $p < 0.05$. $n = 3$ cell pools per group. (For interpretation of the references to colour in this figure legend, the reader is referred to the web version of this article.)

elevated lipid accumulation relative to their corresponding AML-PDCs counterparts (Fig. 6, lowest panel – Oil Red O staining). Same results were obtained when comparing NG and HG conditions of YNG-PDCs to the respective age-matched controls, with a significantly higher lipid accumulation in the former. This evidences the higher adipogenic differentiation capacity of the younger cells, as well as the cells from a diabetic micro-environment. Furthermore, DIO-PDCs in NG conditions showed better chondrogenic differentiation than AML-NG cells. DIO-HG and AML-HG cells did not show significant differences (Fig. 6, lowest panel – Alcian Blue staining). Both NG- and HG-treated YNG-PDCs showed a significantly elevated chondrogenic differentiation capacity when compared to their corresponding AML-PDCs counterparts.

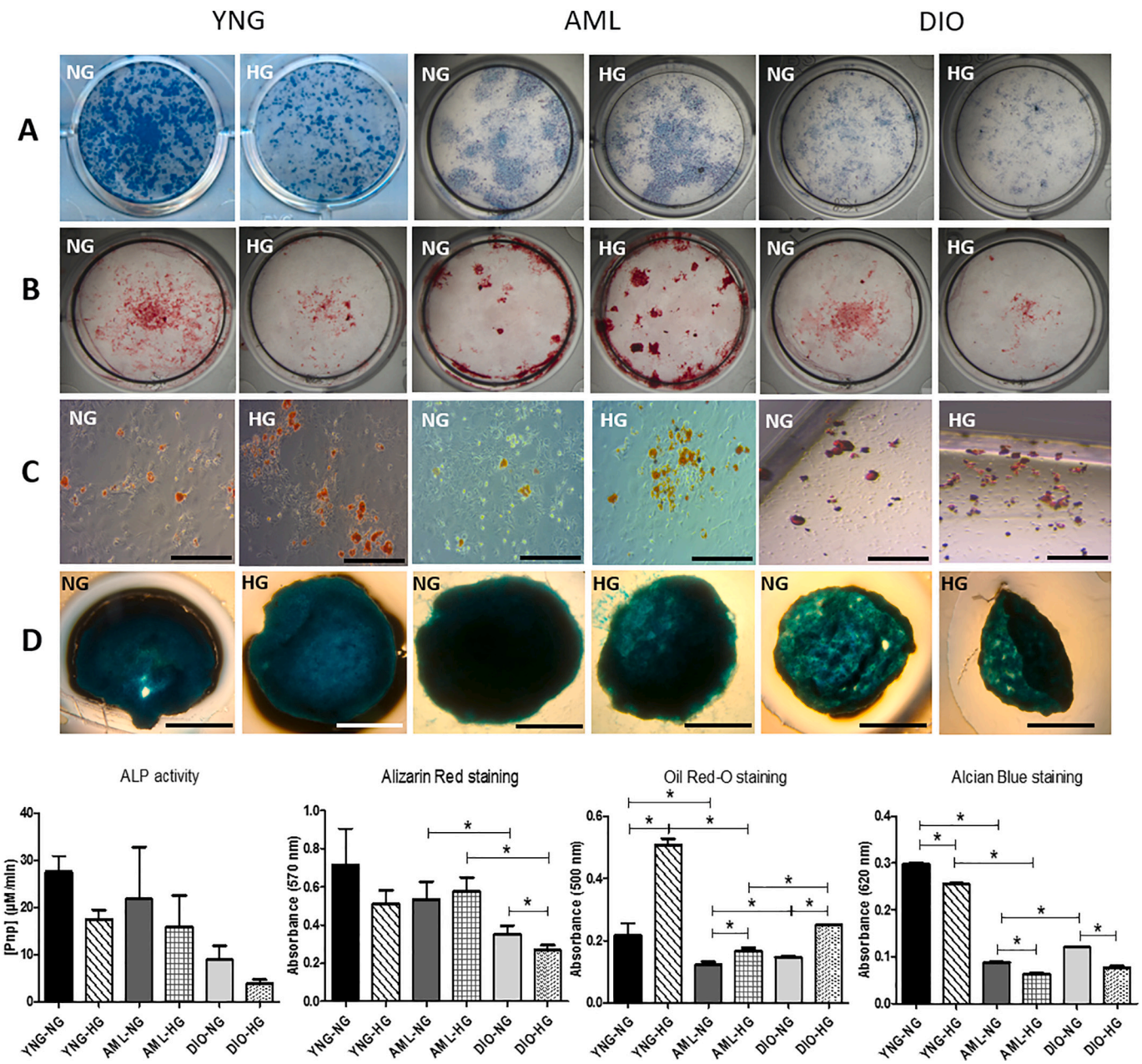


Fig. 6. ALP (row A), Alizarin Red (row B), Oil-Red O (row C) and Alcian Blue (row D) stainings, and their corresponding quantifications (lowest panel), of YNG-, AML- and DIO-PDCs under NG and HG treatments. Timepoint D14 of PDCs differentiation culture for ALP, Alizarin Red and Oil Red-O stainings. Timepoint D28 of µMasses differentiation culture for Alcian Blue staining. Scale bars for row C = 200 µm; for row D = 1 mm. Statistical significance after Bonferroni correction: *$p < 0.007$; $n = 3$–4 cell pools per group. (For interpretation of the references to colour in this figure legend, the reader is referred to the web version of this article.)

3.4. High expression levels of PPARγ and low expression levels of COL2 and COL10 are observed in mPDCs cultured under HG conditions

Gene expression levels of RUNX2 were not significantly different, neither within nor between mice groups (Fig. 7A). On the other hand, HG promoted a significantly elevated expression of PPARγ compared to NG conditions for all groups, except for AML-PDCs (Fig. 7B). Expression levels of SOX9 were modestly decreased by HG in all mice groups, except for the DIO group, which showed a significant decrease of SOX9 expression in HG-treated cells relative to NG-treated cells (Fig. 7C). Furthermore, a significantly decreased expression of chondrogenic marker COL2 was observed for AML-HG and DIO-HG PDCs when compared to their NG counterparts, evidencing the impairment of the chondrogenesis process under a HG micro-environment (Fig. 7D).

PPARγ expression was significantly increased in DIO *vs* AML and YNG *vs* AML cells in HG conditions (Fig. 7B). These data corroborate the results of the lipid accumulation (Fig. 6C and lowest panel – Oil Red O staining). Moreover, no significant differences were observed when comparing the expression of SOX9 between the groups (Fig. 7C). Nonetheless, it is important to note that the increased expression levels of YNG *vs* AML and of AML *vs* DIO in NG conditions were close to statistical significance ($p = 0.0078$ and $p = 0.008$, respectively). Furthermore, DIO-HG cells showed a significantly higher COL2 expression compared to the AML-NG ones (Fig. 7D). Meanwhile, both YNG-NG and YNG-HG cells showed significantly higher expression levels of COL2 when compared to AML-NG and AML-HG counterparts, respectively (Fig. 7D). Expression of the chondrogenic gene MEF2C was significantly decreased in YNG-PDCs cultured in HG conditions relative to YNG-NG,

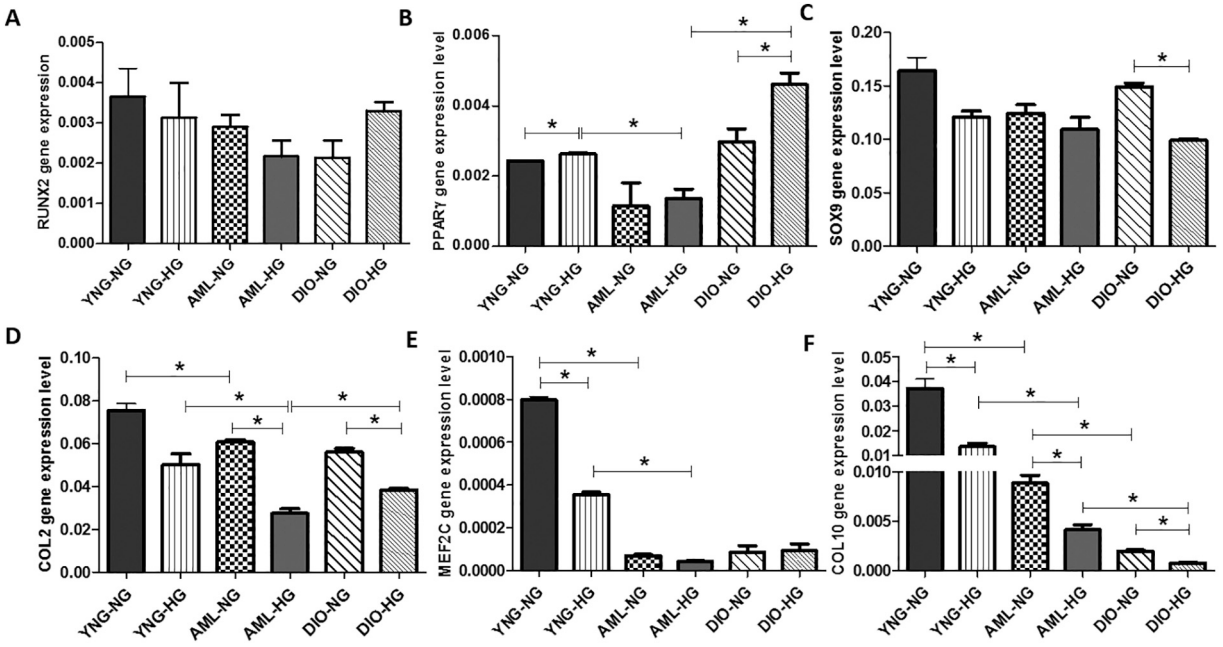


Fig. 7. Gene expression level of A: RUNX2; B: PPARy; C: SOX9; D: COL2; E: MEF2C and F: COL10, from YNG-, AML- and DIO-PDCs, for the assessment of their osteogenic, adipogenic and chondrogenic differentiation under NG and HG treatments. *p < 0.007; n = 3 cell pools per group.

and all AML-PDCs showed a significantly lower MEF2C expression compared to their young counterparts (Fig. 7E). Finally, the HG environment had a negative impact on COL10 expression in all groups of osteochondroprogenitors. YNG-PDCs showed a higher expression level of the chondrogenic gene when compared to AML-PDCs, which likewise presented a higher COL10 expression relative to PDCs from the diabetic micro-environment (Fig. 7F).

3.5. Bone formation and resorption are compromised in DIO mice

Blood serum markers indicative of bone formation and resorption (serum OC and serum CTX, respectively) revealed that the bone turnover process is compromised in the DIO group when compared to age-matched controls. More specifically, OC levels were found significantly decreased (Fig. 8A) and CTX levels significantly increased (Fig. 8B) for DIO mice, relative to AML results. The OC levels of YNG mice point towards significantly more bone formation when compared to the AML group (Fig. 8A), but with unchanged bone resorption, as the level of CTX remained similar between the 2 groups (Fig. 8B).

4. Discussion

The process of bone healing after fracture is a compendium of cellular and molecular events carefully orchestrated to produce a fully loadable, functional, reconstructed bone. However, compromised micro-environments, such as seen in T2DM, affect these events, leading to fracture healing impairment and even non-union [28–30]. Different rodent models have been used to assess the impact that T2DM exerts on bone repair [31–33]. We have used the well-established diet-induced obese (DIO) mouse model, which served as a useful way to mimic and recapitulate the clinical human metabolic derangements. When fed a high-fat diet *ad libitum*, these animals develop obesity, hyperinsulinemia and hyperglycemia, but on the contrary, when fed a normal chow diet they maintain leanness and present no metabolic abnormalities [34]. Our animal model, according to the physiological measurements presented in Fig. 2, reached the T2DM state at 22 weeks of age.

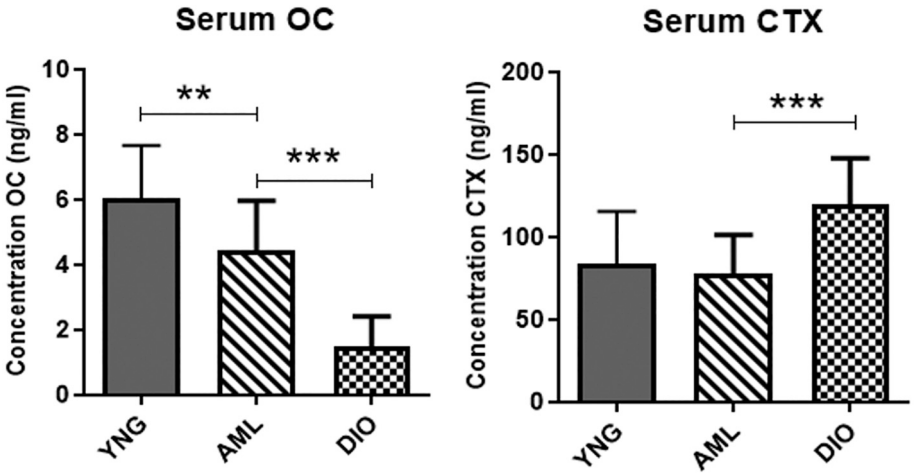


Fig. 8. Blood serum levels of A: OC and B: CTX of YNG, AML and DIO mice, for the assessment of the bone formation and resorption processes, respectively. *p < 0.05; ***p < 0.001; *n* = 11–13 mice per group.

In this study, we have demonstrated that bone fracture healing is impaired in animals under diabetic conditions. Using CE-CT imaging, we were able to simultaneously visualize the different skeletal tissues, and to quantify their amount and spatial distribution. The CE-CT analyses showed that the presence of cartilage (mineralized and unmineralized) in the DIO callus was significantly increased by day 14 post-fracture compared to AML controls. The fact that we were able to discern between bone and mineralized cartilage is of great relevance, since it allowed for the detection of tissue-specific alterations during fracture healing. By solely investigating the total amount of mineralized tissue of the callus, as it is generally reported in literature, the interpretation of results may lack accuracy. Moreover, histological stains for Alcian Blue and Masson Trichrome allowed us to validate the CE-CT results, thereby evidencing the value of CE-CT for visualization and quantification of tissues of interest. By generating 3D CE-CT renderings, the impairment in the repair of the DIO fracture relative to the AML group was revealed. The observed exacerbated presence of cartilage tissue in the DIO callus compared to the AML callus 14 days post-trauma suggests that either the process of cartilage formation or the process of cartilage turnover, the latter dictating the transition from mineralized cartilage to woven bone, is impaired in DIO mice and may represent evidence of a slower fracture healing process. Additionally, simultaneous visualization of both unmineralized and mineralized cartilage *via* CE-CT revealed that these tissues had already almost disappeared in YNG fracture calluses when compared to AML mice. This suggests that ageing is affecting the bone repair at this stage of the process. It is important to clarify that it was not the aim of this study to investigate the characteristics of "aged" or "geriatric" bones during fracture healing. Geriatric murine bones are usually reported in literature for mice from 12-months old onwards [35,36]. Instead, the inclusion of the YNG group aimed at accurately discerning between the full impact of a diabetic state and the impact of ageing (at the 22-weeks old timepoint, age-matched to our DIO mice group) on bone tissue. Furthermore, the fracture callus of the YNG mice was found to have more trabecular bone-like structures than the age-matched controls. Blood serum OC levels correspond with this increased volume of newly-formed bone seen in YNG callus compared to the age-matched controls, further confirming a slower bone repair due to ageing in AML animals. These results agree with previous studies on geriatric rodents, which have shown decreased bone formation, delayed cartilage resorption and slower mineralization of the fracture callus [35,37–39], all in concordance with the characteristics of our AML mice compared to YNG ones. Additionally, OC results from a previous study of our group also evidenced elevated bone formation occurring in YNG mice compared to AML [26]. In contrast, previous CTX results differ from our current study, which reports unchanged levels of the biomarker between both groups. It should be highlighted though that the bone turnover results from our previous study were obtained from non-fractured animals.

Furthermore, we observed a tendency to a higher callus volume and lower BV/TV in the DIO callus compared to AML controls. The latter result matches with the findings of the study of Brown et al. [6], which also showed a decrease in callus bone volume of HFD-fed mice by day 14 post-fracture compared to lean animals, with a continued decline until day 21 [6]. The dynamics of the fracture healing process over time is precisely one limitation of our study. The evaluation of multiple timepoints could give more insight into the differences of the various skeletal tissues assessed between T2DM and healthy subjects, and could define, for example, the approximate timepoint when the repair process starts being delayed in T2DM.

Significantly higher expression of CTX and lower expression of OC in DIO animals compared to AML controls evidence a compromised bone turnover, resulting ultimately in the loss of bone volume. This explains the lower BV/TV observed in DIO bone relative to the age-matched controls at day 14 post-fracture and suggests that the BV/TV difference reaches statistical significance at a later timepoint, analogous to the study of Brown et al. [6]. Similar to our study, Picke et al. [40] assessed bone formation and resorption by evaluating serum type 1 procollagen amino-terminal-propeptide (P1NP) and CTX levels in T2DM rats after subcritical femoral fracture. The authors showed that, when compared to lean controls, bone formation was suppressed while bone resorption was favored in T2DM animals [40], in line with the results of our study.

It is important to take into account that, contrary to observations in rodents, most studies assessing bone turnover in human subjects suffering from T2DM reported both decreased bone formation and decreased bone resorption biomarker levels (*i.e.* decreased bone turnover) [41–43]. More investigations regarding formation and resorption during bone repair in T2DM patients are needed to clearly establish the differences between humans and animals in the bone turnover process and how far bone fracture healing is reflected in systemic bone turnover parameters process.

Another finding obtained from the CE-CT results was an increased presence of adipose tissue in the fracture callus of the DIO mice. Once again, our results are in line with those of Brown et al., who observed that peripilin and PPARγ expression, two known biomarkers of adipogenic differentiation, were increased in the fracture callus of obese mice compared to controls [6]. Thanks to the use of CE-CT, we were able to report this result for the first time in 3D in a DIO mouse model of bone fracture healing.

It has been reported that mesenchymal stem cells and osteoprogenitors located in the periosteum (PDCs) play a key role in the fracture healing process [23,24]. In this sense, we characterized PDCs isolated from YNG, AML and DIO bones under hyperglycemic and normoglycemic *in vitro*. In line with what was previously discussed, adipogenic differentiation was significantly increased in diabetic periosteal cells after 14 days of HG culture compared to NG-treated cells. The elevated PPARγ expression of the former confirmed this result. The notable difference of both PPARγ expression levels and lipid accumulation between DIO- and AML-PDCs seen *in vitro* correlates with our *in vivo* findings, where the volume of adipocytes in the DIO callus was significantly higher when compared to age-matched controls. This confirms that HG in T2DM conditions promotes adipogenic differentiation and, thus, increases adipocyte presence in the callus during the fracture healing process. A study supporting our findings is the one of Devlin et al. [7], in which a 2-fold increase of the adipocyte ratio in the bone marrow of the long bones from DIO mice compared to lean controls was observed [7]. Similarly, Scheller et al. [44] reported higher marrow adipose tissue volume in the tibia of obese animals subject to 16 weeks of HFD treatment, and the prevention of the marrow adipose tissue expansion by means of weight loss [44]. On the other hand, Alizarin Red and ALP assays showed compromised osteoblastic differentiation when diabetic osteoprogenitors were cultured in HG conditions. In addition, AML-PDCs cultured in normoglycemia showed a better osteogenic performance compared to DIO osteoprogenitors, further evidencing that the diabetic micro-environment promotes osteoblastic dysfunctionality of PDCs. Consequently, the observed hindered osteoblast differentiation of diabetic osteoprogenitors, their increased adipogenesis and the evidence of exacerbated presence of adipocytes *in vivo* in the fracture callus of DIO mice suggest that the impairment of the bone repair process is, at least partly, due to a preference in the differentiation fate of the PDCs from the osteogenic to the adipogenic lineage. This hypothesis has been discussed previously by other authors, stating that the diminished functional osteoblastic population due to the preferred adipogenic differentiation pathway cannot sustain properly the bone formation process, ultimately resulting in impaired fracture healing [6,8]. These findings, coupled with the overall decrease in viability and proliferation of cells under HG conditions *in vitro*, can explain the difficulty that osteochondroprogenitors experience for contributing to an effective bone repair in T2DM conditions.

Furthermore, the HG-mediated impaired chondrogenic differentiation of mPDCs was evident after Alcian Blue and gene expression assays, in particular for the diabetic osteochondroprogenitors, which showed significantly decreased expression of SOX9, COL2 and COL10 genes

when compared to their normoglycemic-treated counterparts. This compromised chondrogenesis of the diabetic periosteal cells *in vitro* can be related to the accumulation of cartilage *in vivo,* as observed by CE-CT. The low expression levels of SOX9 and COL2 of these progenitors reflect the delayed process of cartilage formation during earlier timepoints of the bone repair. Thus, cartilaginous tissue accumulates at day 14 post-fracture, when the process of cartilage maturation and resorption might still not have started or be as advanced as in the control group. Indeed, the low expression levels of COL10 in hyperglycemic DIO-PDCs relative to their normoglycemic counterparts evidences that maturation of the chondrocytes to achieve hypertrophy is compromised [45,46], thus further impeding the formation of more mineralized bone in the DIO callus 14 days after fracture. The fact that DIO-PDCs have a significantly lower expression of COL10 compared to AML-PDCs suggests that the progenitor cells in the DIO callus go through a slower chondrogenic differentiation, consequently delaying the fracture healing process, in line with our *in vivo* CE-CT results. Nevertheless, it is necessary to reiterate that our *in vivo* results are the representation of the state of bone repair specifically at day 14 post-fracture. With this in mind, alterations of the chondrogenic process in the diabetic periosteal cells can still impair bone healing at other timepoints. As stated before, the study of the dynamics of the fracture healing process would be very insightful to elucidate the timeline of the T2DM bone pathology. Another study has also confirmed that DIO mice exhibit delayed fracture healing, due to aberrations with the collagen [47]. The authors found that the DIO callus showed accumulation of advanced glycation end products (AGEs) and collagen I fibers that are notably sparse with an abnormal microstructure, all favoring defective callus mineralization, remodeling and strength. Part of these findings are supported by a previous study from our group [48], in which AGEs were found to be accumulated in the long bones of DIO mice, when compared to lean controls.

The clear contrast in differentiation potential between younger and older periosteal cells for osteogenesis, adipogenesis and chondrogenesis strongly suggests that an impairment in fracture healing can be associated with age-related changes occurring in these progenitor cells. In literature, it has been reported that cellular senescence is increased in skeletal stem cells under ageing and hyperglycemic conditions [49,50]. For example, studies have shown how cell number and functionality were significantly compromised due to age-associated inflammation regulated by NF-κB and TNFα, triggered by increased cell senescence [33,51]. Specifically in the study from Josephson et al. [51], skeletal stem cells exposed to an age-associated local proinflammatory microenvironment showed a decrease in osteogenic differentiation and an increase in adipogenic differentiation [51]. These outcomes likely contributed to hindering the bone healing process, similar to our study conclusions. On the other hand, different studies have indicated that HG induced local inflammation and senescence on skeletal stem cells primarily mediated *via* the Akt/mTOR signaling pathway and autophagic processes, thus explaining the impaired skeletal cell functionality and number in diabetic rodents [52,53].

Compromised cell behavior of chondroprogenitor cells due to ageing has also been reported previously. A study from Lopas et al. showed decreased proliferation of aged osteo- and chondroprogenitor cells associated with a decrease in bone and cartilage content within the fracture callus of geriatric mice compared to young controls [35]. Moreover, another study reported that the osteogenic differentiation and osteocalcin expression were delayed in PDCs from the fracture site of middle-aged adult mice, compared to their young counterparts [36], the former of comparable age relative to our AML mice. Similar to our study, the authors found a low expression of COL2 in aged murine progenitor cells, and delayed cartilage matrix deposition during fracture healing, when compared to young animals [36]. Meanwhile, impairment of chondrogenesis in progenitor cells due to the diabetic microenvironment has been assessed previously in a study by Tevlin et al. [33]. The authors reported that Indian hedgehog (Ihh) expression, a key factor for endochondral ossification and cartilage development [54], was decreased in mouse skeletal stem cells isolated from diabetic animals [33]. It was observed that when the hedgehog signaling was suppressed during femoral fracture healing of diabetic mice, the expansion of the skeletal stem cells was inhibited, generating bone repair impairment. Subsequently, it was demonstrated that the rescue of the fracture healing process was possible after delivering purified Ihh to the fracture site [33]. Other study (Wu et al., 2013) has also found compromised chondrogenesis in different stem cells isolated from obese mice [55]. In the present study, chondrogenic differentiation measured through Alcian Blue staining was found significantly increased for DIO-PDCs when compared to AML controls, seemingly contradicting the results mentioned from previous studies. It is important to note though that this significant difference is present only when comparing progenitors cultured in NG conditions, and in the work from Wu et al. only a model of HG-cultured stem cells was used. Our finding may suggest the possibility that the differentiation in the NG micro-environment is favoring the rescue of the chondrogenesis process in the DIO-PDCs, since also all chondrogenic markers measured (except COL10) show similar expression levels between DIO and control cells. Nevertheless, more *in vitro* experimentation with osteochondroprogenitors isolated from the diabetic micro-environment will be necessary in the future to clarify these outcomes.

Overall, our results suggest that the impairment of the bone fracture healing process is closely related to impaired differentiation of chondro- and osteoprogenitor cells promoted by hyperglycemia in T2DM conditions.

5. Conclusion

In this study, we have demonstrated that T2DM exerts a negative impact on bone fracture healing. Simultaneous quantification of the different tissues involved in bone fracture healing, *i.e.* bone, unmineralized and mineralized cartilage and adipose tissue, by CE-CT revealed alterations in tissue ratios not only in diabetic, but also in ageing conditions. Particularly, we were able to differentiate within the fracture callus between newly-formed bone tissue and mineralized cartilage, showing the added value of the CE-CT technique in bone research. Evidence of fracture healing delay was documented by the elevated amount of cartilaginous tissue in the fracture callus of DIO mice compared to controls at 14 days post-fracture. The exacerbated presence of cartilage by this timepoint in the DIO callus can be related to impaired chondrogenic differentiation of PDCs of HG-treated cells compared to NG-treaded cells. In addition, cell differentiation of PDCs favoring the adipogenic lineage at the expense of the osteoblastic lineage was observed, possibly resulting in a significant smaller amount of woven bone illustrative for fracture healing delay. The bone repair process may be further impaired by alterations in bone turnover in both ageing and diabetic mice, but especially for the latter, which showed lower levels of bone formation (OC) and higher levels of bone resorption (CTX) when compared to controls. Further investigations should focus on the callus vascularization and inflammation markers, to elucidate other pathophysiological mechanisms involved in fracture healing under T2DM conditions.

CRediT authorship contribution statement

Authors' roles: Study design: CM, GK, KV. Study conduct: CM. Data collection: CM. Data analysis: CM, JT. Data interpretation: CM, GK. Drafting manuscript: CM. Revising manuscript content: CM, JT, FPL, KV, GK. Approving final version of manuscript: CM, JT, FPL, KV, GK. CM takes full responsibility for the integrity of the data analysis.

Declaration of competing interest

None.

Acknowledgements

This work is part of Prometheus, the KU Leuven R&D Division for Skeletal Tissue Engineering: www.kuleuven.be/prometheus. The research leading to these results has received funding from: i) the European Research Council under the European Union's Seventh Framework Programme (FP/2007-2013)/ERC Grant Agreement no 249191; ii) the special research fund of the KU Leuven (GOA/13/016) and iii) the Belgian Research Foundation Flanders (FWO, Grant No. G088218N). The statistical analysis of the *in vitro* studies was done under the counselling of Annouschka Laenen from the Biostatistics and Statistical Bioinformatics Center (L-BioStat) of the KU Leuven. The CE-CT images have been generated at the X-ray computed tomography facilities of the Department of Development and Regeneration of the KU Leuven, financed by the Hercules Foundation (project AKUL 13/47). Histological stains and images were performed and acquired by Michele de Beukelaer from the IREC Imaging Platform (2IP) of the UCLouvain, Belgium.

References

[1] L. Claes, S. Recknagel, A. Ignatius, Fracture healing under healthy and inflammatory conditions, Nat. Rev. Rheumatol. Nature Publishing Group 8 (3) (2012) 133–143.
[2] C.D. Mathers, D. Loncar, Projections of global mortality and burden of disease from 2002 to 2030, PLoS Med. 3 (11) (2006) 2011–2030.
[3] S. Cernea, M. Dobreanu, Diabetes and beta cell function: From mechanisms to evaluation and clinical implications, Biochem. Medica. (2013) 266–280.
[4] B. Roy, Biomolecular basis of the role of diabetes mellitus in osteoporosis and bone fractures, World J. Diabetes 4 (4) (2013) 101–113.
[5] M. Saito, K. Fujii, Y. Mori, K. Marumo, Role of collagen enzymatic and glycation induced cross-links as a determinant of bone quality in spontaneously diabetic WBN/Kob rats, Osteoporos. Int. 17 (10) (2006) 1514–1523.
[6] M.L. Brown, K. Yukata, C.W. Farnsworth, D.-G. Chen, H. Awad, M.J. Hilton, R. J. O'Keefe, L. Xing, R.A. Mooney, M.J. Zuscik, Delayed fracture healing and increased callus adiposity in a C57BL/6J murine model of obesity-associated type 2 diabetes mellitus, PLoS One 9 (6) (2014), e99656.
[7] M.J. Devlin, A. Robbins, M.N. Cosman, C.A. Moursi, A.M. Cloutier, L. Louis, M. Van Vliet, C. Conlon, M.L. Bouxsein, Differential effects of high fat diet and diet-induced obesity on skeletal acquisition in female C57BL/6J vs. FVB/NJ mice, Bone Rep. 8 (2018) 204–214.
[8] C. Hamann, C. Goettsch, J. Mettelsiefen, V. Henkenjohann, M. Rauner, U. Hempel, R. Bernhardt, N. Fratzl-Zelman, P. Roschger, S. Rammelt, K.-P. Gunther, L. C. Hofbauer, Delayed bone regeneration and low bone mass in a rat model of insulin-resistant type 2 diabetes mellitus is due to impaired osteoblast function, AJP Endocrinol. Metab. 301 (17) (2011) E1220–E1228.
[9] M. Tencerova, F. Figeac, N. Ditzel, H. Taipaleenmäki, T.K. Nielsen, M. Kassem, High-fat diet–induced obesity promotes expansion of bone marrow adipose tissue and impairs skeletal stem cell functions in mice, J. Bone Miner. Res. 33 (6) (2018) 1154–1165.
[10] T. Vehmas, K.J. Kairemo, M.J. Taavitsainen, Measuring visceral adipose tissue content from contrast enhanced computed tomography, Int. J. Obes. Relat. Metab. Disord. 20 (6) (1996) 570–573.
[11] R.M. Schultz, E.R. Wisner, E.G. Johnson, J.S. MacLeod, Contrast-enhanced computed tomography as a preoperative indicator of vascular invasion from adrenal masses in dogs, Vet. Radiol. Ultrasound. 0 (6) (2009) 625–629.
[12] H.J. Nieminen, T. Ylitalo, S. Karhula, J.P. Suuronen, S. Kauppinen, R. Serimaa, E. Hæggström, K.P.H. Pritzker, M. Valkealahti, P. Lehenkari, M. Finnilä, S. Saarakkala, Determining collagen distribution in articular cartilage using contrast-enhanced micro-computed tomography, Osteoarthr. Cartil. 23 (9) (2015) 1613–1621.
[13] S. De Bournonville, S. Vangrunderbeeck, G. Kerckhofs, Contrast-enhanced microCT for virtual 3D anatomical pathology of biological tissues: a literature review, Contrast Media Mol. Imaging. 2019 (2019) 8617406.
[14] G. Kerckhofs, J. Sainz, M. Maréchal, M. Wevers, T. Van de Putte, L. Geris, J. Schrooten, Contrast-enhanced nanofocus X-ray computed tomography allows virtual three-dimensional histopathology and morphometric analysis of osteoarthritis in small animal models, Cartilage. 5 (1) (2014) 55–65.
[15] G. Kerckhofs, S. Stegen, N. van Gastel, A. Sap, G. Falgayrac, G. Penel, M. Durand, F. P. Luyten, L. Geris, K. Vandamme, T. Parac-Vogt, G. Carmeliet, Simultaneous three-dimensional visualization of mineralized and soft skeletal tissues by a novel microCT contrast agent with polyoxometalate structure, Biomaterials. 159 (2018) 1–12.
[16] R.T. Branca, A. McCallister, H. Yuan, A. Aghajanian, J.E. Faber, N. Weimer, R. Buchanan, C.S. Floyd, M. Antonacci, L. Zhang, A. Burant, Accurate quantification of brown adipose tissue mass by xenon-enhanced computed tomography, Proc. Natl. Acad. Sci. 115 (1) (2018) 174–179.
[17] A. Gandhi, C. Dumas, J.P. O'Connor, J.R. Parsons, S.S. Lin, The effects of local platelet rich plasma delivery on diabetic fracture healing, Bone. 38 (4) (2006) 540–546.
[18] B. Cao, N. Liu, W. Wang, High glucose prevents osteogenic differentiation of mesenchymal stem cells via lncRNA AK028326/CXCL13 pathway, Biomed. Pharmacother. 84 (2016) 544–551.
[19] J. Wang, B. Wang, Y. Li, D. Wang, E. Lingling, Y. Bai, H. Liu, High glucose inhibits osteogenic differentiation through the BMP signaling pathway in bone mesenchymal stem cells in mice, EXCLI J. 12 (2013) 584–597.
[20] Y. Zhang, J.H. Yang, Activation of the PI3K/Akt pathway by oxidative stress mediates high glucose-induced increase of adipogenic differentiation in primary rat osteoblasts, J. Cell. Biochem. 114 (11) (2013) 2595–2602.
[21] S. Ehnert, T. Freude, C. Ihle, L. Mayer, B. Braun, J. Graeser, I. Flesch, U. Stöckle, A. K. Nussler, S. Pscherer, Factors circulating in the blood of type 2 diabetes mellitus patients affect osteoblast maturation - description of a novel in vitro model, Exp. Cell Res. 332 (2) (2014) 1–12.
[22] C.-C. Guan, M. Yan, X.-Q. Jiang, P. Zhang, X.-L. Zhang, J. Li, D.-X. Ye, F.-Q. Zhang, Sonic hedgehog alleviates the inhibitory effects of high glucose on the osteoblastic differentiation of bone marrow stromal cells, Bone. 45 (6) (2009) 1146–1152.
[23] E.J. Arnsdorf, L.M. Jones, D.R. Carter, C.R. Jacobs, The periosteum as a cellular source for functional tissue engineering, Tissue Eng. Part A. 15 (9) (2009) 2637–2642.
[24] N. Van Gastel, S. Torrekens, S.J. Roberts, K. Moermans, J. Schrooten, P. Carmeliet, A. Luttun, F.P. Luyten, G. Carmeliet, Engineering vascularized bone: Osteogenic and proangiogenic potential of murine periosteal cells, Stem Cells 30 (11) (2012) 2460–2471.
[25] N. Otsu, A threshold selection method from gray-level histograms, IEEE Trans. Syst. Man. Cybern. 9 (1) (1979) 62–66.
[26] G. Kerckhofs, M. Durand, R. Vangoitsenhoven, C. Marin, B. Van der Schueren, G. Carmeliet, F.P. Luyten, L. Geris, K. Vandamme, Changes in bone macro- and microstructure in diabetic obese mice revealed by high resolution microfocus X-ray computed tomography, Sci. Rep. 6 (September) (2016) 1–13.
[27] L.F. Mendes, K. Bosmans, I. Van Hoven, S.R. Viseu, M. Maréchal, F.P. Luyten, Developmental engineering of living implants for deep osteochondral joint surface defects, Bone. 139 (2020) 115520.
[28] C. Hamann, S. Kirschner, K.-P. Günther, L.C. Hofbauer, Bone, sweet bone—osteoporotic fractures in diabetes mellitus, Nat. Rev. Endocrinol. 8 (5) (2012) 297–305.
[29] J.W. Folk, A.J. Starr, J.S. Early, Early wound complications of operative treatment of calcaneus fractures: analysis of 190 fractures, J. Orthop. Trauma 13 (5) (1999) 369–372.
[30] R.T. Loder, The influence of diabetes mellitus on the healing of closed fractures, Clin. Orthop. Relat. Res. 232 (1988) 210–216.
[31] C. Hamann, A.-K. Picke, G.M. Campbell, M. Balyura, M. Rauner, R. Bernhardt, G. Huber, M.M. Morlock, K.-P. Günther, S.R. Bornstein, C.-C. Glüer, B. Ludwig, L. C. Hofbauer, Effects of parathyroid hormone on bone mass, bone strength, and bone regeneration in male rats with type 2 diabetes mellitus, Endocrinology. 155 (4) (2014) 1197–1206.
[32] C. Wallner, J. Schira, J.M. Wagner, M. Schulte, S. Fischer, T. Hirsch, W. Richter, S. Abraham, U. Kneser, M. Lehnhardt, B. Behr, Application of VEGFA and FGF-9 enhances angiogenesis, osteogenesis and bone remodeling in type 2 diabetic long bone regeneration, PLoS One 10 (3) (2015), e0118823.
[33] R. Tevlin, E.Y. Seo, O. Marecic, A. McArdle, X. Tong, B. Zimdahl, A. Malkovskiy, R. Sinha, G. Gulati, X. Li, T. Wearda, R. Morganti, M. Lopez, R.C. Ransom, C. R. Duldulao, M. Rodrigues, A. Nguyen, M. Januszyk, Z. Maan, K. Paik, K.S. Yapa, J. Rajadas, D.C. Wan, G.C. Gurtner, M. Snyder, P.A. Beachy, F. Yang, S. B. Goodman, I.L. Weissman, C.K.F. Chan, M.T. Longaker, Pharmacological rescue of diabetic skeletal stem cell niches, Sci. Transl. Med. 9 (372) (2017).
[34] C.-Y. Wang, J.K. Liao, A mouse model of diet-induced obesity and insulin resistance, Methods Mol. Biol. 821 (2012) 421–433.
[35] L.A. Lopas, N.S. Belkin, P.L. Mutyaba, C.F. Gray, K.D. Hankenson, J. Ahn, Fractures in geriatric mice show decreased callus expansion and bone volume, Clin. Orthop. Relat. Res. 472 (11) (2014) 3523–3532.
[36] C. Lu, T. Miclau, D. Hu, E. Hansen, K. Tsui, C. Puttlitz, R.S. Marcucio, Cellular basis for age-related changes in fracture repair, J. Orthop. Res. 3 (6) (2005) 1300–1307.
[37] R.A. Meyer, P.J. Tsahakis, D.F. Martin, D.M. Banks, M.E. Harrow, G.M. Kiebzak, Age and ovariectomy impair both the normalization of mechanical properties and the accretion of mineral by the fracture callus in rats, J. Orthop. Res. 19 (3) (2001) 428–435.
[38] B. Bak, T. Andreassen, The effect of aging on fracture healing in the rat, Calcif. Tissue Int. 45 (5) (1989) 292–297.
[39] D. Clark, M. Nakamura, T. Miclau, R. Marcucio, Effects of aging on fracture healing, Curr. Osteoporos. Rep. 15 (6) (2017) 601–608.
[40] A.K. Picke, J. Salbach-Hirsch, V. Hintze, S. Rother, M. Rauner, C. Kascholke, S. Möller, R. Bernhardt, S. Rammelt, M.T. Pisabarro, G. Ruiz-Gómez, M. Schnabelrauch, M. Schulz-Siegmund, M.C. Hacker, D. Scharnweber, C. Hofbauer, L.C. Hofbauer, Sulfated hyaluronan improves bone regeneration of diabetic rats by binding sclerostin and enhancing osteoblast function, Biomaterials. 96 (2016) 11–23.
[41] J.O.B. Madsen, C.W. Herskin, B. Zerahn, N.R. Jørgensen, B.S. Olsen, F. Pociot, J. Johannesen, Decreased markers of bone turnover in children and adolescents with type 1 diabetes, Pediatr. Diabetes 21 (3) (2020) 505–514.
[42] G. Colleluori, L. Aguirre, R. Dorin, D. Robbins, D. Blevins, Y. Barnouin, R. Chen, C. Qualls, D.T. Villareal, R. Armamento-Villareal, Hypogonadal men with type 2 diabetes mellitus have smaller bone size and lower bone turnover, Bone. 99 (2017) 14–19.
[43] M.R. Rubin, Bone cells and bone turnover in diabetes mellitus, Curr. Osteoporos. Rep. 13 (3) (2015) 186–191.

[44] E.L. Scheller, B. Khoury, K.L. Moller, N.K.Y. Wee, S. Khandaker, K.M. Kozloff, S. H. Abrishami, B.F. Zamarron, K. Singer, Changes in skeletal integrity and marrow adiposity during high-fat diet and after weight loss, Front. Endocrinol. (Lausanne) 7 (2016) 102.
[45] C. Lu, T. Miclau, D. Hu, R.S. Marcucio, Ischemia leads to delayed union during fracture healing: a mouse model, J. Orthop. Res. 25 (1) (2007) 51–61.
[46] P. Wang, J. Ying, C. Luo, X. Jin, S. Zhang, T. Xu, L. Zhang, M. Mi, D. Chen, P. Tong, H. Jin, Osthole promotes bone fracture healing through activation of bmp signaling in chondrocytes, Int. J. Biol. Sci. 13 (8) (2017) 996–1007.
[47] D.K. Khajuria, M. Soliman, J.C. Elfar, G.S. Lewis, T. Abraham, F. Kamal, R. A. Elbarbary, Aberrant structure of fibrillar collagen and elevated levels of advanced glycation end products typify delayed fracture healing in the diet-induced obesity mouse model, Bone. 137 (2020) 115436.
[48] C. Marin, G. Papantonakis, K. Sels, G.H. van Lenthe, G. Falgayrac, R. Vangoitsenhoven, B. Van der Schueren, G. Penel, F. Luyten, K. Vandamme, G. Kerckhofs, Unraveling the compromised biomechanical performance of bone in type 2 diabetes- and Roux-en-Y gastric bypass mice by linking the mechanical-structural and physico-chemical properties, Sci. Rep. 8 (1) (2018) 5881.
[49] I. Bellantuono, A. Aldahmash, M. Kassem, Aging of marrow stromal (skeletal) stem cells and their contribution to age-related bone loss, Biochim. Biophys. Acta Mol. basis Dis. 792 (4) (2009) 364–370.
[50] T.H. Ambrosi, L.H. Goodnough, C.K.F. Chan, Human skeletal stem cell aging, Aging (Albany NY) 12 (17) (2020) 16669–16671.
[51] A.M. Josephson, V. Bradaschia-Correa, S. Lee, K. Leclerc, K.S. Patel, E.M. Lopez, H. P. Litwa, S.S. Neibart, M. Kadiyala, M.Z. Wong, M.M. Mizrahi, N.L. Yim, A. J. Ramme, K.A. Egol, P. Leucht, Age-related inflammation triggers skeletal stem/progenitor cell dysfunction, Proc. Natl. Acad. Sci. U. S. A. 116 (14) (2019) 6995–7004.
[52] D. Zhang, H. Lu, Z. Chen, Y. Wang, J. Lin, S. Xu, C. Zhang, B. Wang, Z. Yuan, X. Feng, X. Jiang, J. Pan, High glucose induces the aging of mesenchymal stem cells via Akt/mTOR signaling, Mol. Med. Rep. 16 (2) (2017) 1685–1690.
[53] T.C. Chang, M.F. Hsu, K.K. Wu, High glucose induces bone marrow-derived mesenchymal stem cell senescence by upregulating autophagy, PLoS One 10 (5) (2015), e0126537.
[54] M.J. Hilton, Ihh controls cartilage development by antagonizing Gli3, but requires additional effectors to regulate osteoblast and vascular development, Development. 132 (19) (2005) 4339–4351.
[55] C.L. Wu, B.O. Diekman, D. Jain, F. Guilak, Diet-induced obesity alters the differentiation potential of stem cells isolated from bone marrow, adipose tissue and infrapatellar fat pad: the effects of free fatty acids, Int. J. Obes. 37 (8) (2013) 1079–1087.